

A Dual-Network Model of Pore Structure for Vuggy Carbonates

M.A. Ioannidis and I. Chatzis
Porous Media Research Institute
Department of Chemical Engineering
University of Waterloo, Ontario, Canada

Abstract

A dual-network model of the pore structure of vuggy carbonates is introduced and studied. The model combines small-scale pore structure information (porosity and pore size distribution) pertaining to the matrix, with X-ray CT porosity distributions, which provide information about secondary porosity at the scale of several millimeters (large scale). The dual network accounts for partial connectivity of and local constrictions in the secondary pore space. The model is constructed by superimposing vugs on blocks of matrix in agreement with a given porosity distribution. Core analysis results qualitatively support the new model as a tool to interpret the diverse transport and capillary behavior of vuggy carbonates.

Introduction

Wide variability in the amount, the size distribution and, especially, the degree of interconnectedness of secondary porosity (vugs and solution channels) seriously complicates the interpretation of core analysis data from carbonate rocks. Pore-scale network simulation, which has proven useful in relating pore structure parameters to various petrophysical properties of relatively homogeneous sandstones (*e.g.*, Ioannidis and Chatzis, 1993), has not been adequately extended to vuggy carbonates. Efforts to model secondary porosity in vuggy carbonates in terms of a swarm of spherical cavities of uniform size imbedded in porous matrix are inadequate for two reasons. Not only is secondary porosity in carbonate rocks broadly distributed and spatially correlated (Hicks *et al.*, 1992), but most importantly, vugs and solution channels often form a partially interconnected secondary network (Gleeson, 1993). A major implication of the latter fact is that accessibility of the secondary pore space to a non-wetting phase is not exclusively controlled by matrix properties. As a result, important petrophysical properties dependent on fluid distribution within the pore space (capillary pressure, resistivity index and relative permeability curves) exhibit widely diverse behavior that is difficult to predict.

Explicit representation of the structure of vuggy carbonates as a single pore network (Kamath *et al.*, 1998) is of little value if the characteristic sizes of matrix (intergranular/intercrystalline) and secondary (vugs, solution channels) pores are very different. Alternatively, such media may be conceptually described as a dual network,

consisting of a partially interconnected network of vug pore bodies communicating through vug pore throats, superimposed on a fully interconnected network of matrix pore bodies and pore throats that may be treated as a continuum. The distinction between vug and matrix pores and throats is made simply on the basis of relative size. Such a description is, however, confronted with lack of information regarding the size distributions of vug pore bodies and throats, and the degree of interconnectedness of their network. Unlike matrix pore networks, which have been extensively studied using mercury porosimetry and image analysis, the investigation of secondary pore space has been largely limited to the measurement of vug porosity using X-ray computed tomography. The extent of vug communication is still poorly understood (Lucia, 1983) and the size distribution of constrictions in the secondary pore space (vug pore throats) is unknown. Notwithstanding these problems, consistent formulation of a dual-network model is still possible by capitalizing on existing information as explained next.

Dual-network Model Formulation

Consider a cubic tessellation of a vuggy porous medium of size L into a number of blocks of size l , which may contain both matrix and vuggy porosity. Matrix permeability k_m and porosity ϕ_m may be distributed in these blocks in a correlated or uncorrelated fashion (Ioannidis *et al.*, 1996). In this paper we assume for simplicity that matrix properties are uniform and known from small-scale investigations (*e.g.*, analysis of thin-section images). In order to construct a dual-network model, information about the secondary pore system must also be included. Rudimentary information is contained in the value of local vuggy porosity $\phi_v(\mathbf{x})$, where \mathbf{x} is the position vector. We assume that this property is distributed in blocks of size l according to a known distribution function.

A simple and rational way to account for possible communication between vugs in neighboring blocks located at points \mathbf{x} and \mathbf{x}^* , is to assume that the probability of finding a connection between them, denoted by $p(\mathbf{x}, \mathbf{x}^*)$, is proportional to the product of local vug porosity values, $\phi_v(\mathbf{x})$ and $\phi_v(\mathbf{x}^*)$. This probability may be expressed as follows:

$$p(\mathbf{x}, \mathbf{x}^*) = [\phi_v(\mathbf{x})\phi_v(\mathbf{x}^*)]^{(1-\omega)/\omega} \quad ; \quad 0 \leq \omega \leq 1 \quad (1)$$

Accordingly, if either $\phi_v(\mathbf{x})$ or $\phi_v(\mathbf{x}^*)$ is equal to zero, block communication through secondary porosity is impossible and, if both $\phi_v(\mathbf{x})$ and $\phi_v(\mathbf{x}^*)$ are equal to one, block communication through secondary porosity is certain. The parameter ω controls the strength of the probability for $0 < \phi_v(\mathbf{x})\phi_v(\mathbf{x}^*) < 1$. Thus, $p(\mathbf{x}, \mathbf{x}^*) \rightarrow 0$ as $\omega \rightarrow 0$ (completely disconnected secondary porosity), and $p(\mathbf{x}, \mathbf{x}^*) \rightarrow 1$ as $\omega \rightarrow 1$ (fully connected secondary porosity).

In order to permit calculations of transport and capillary properties at the block scale, additional assumptions about the vug geometry at this scale are needed. Consider a cubic block of volume l^3 located at point \mathbf{x} and filled with porous matrix. Inside the cubic

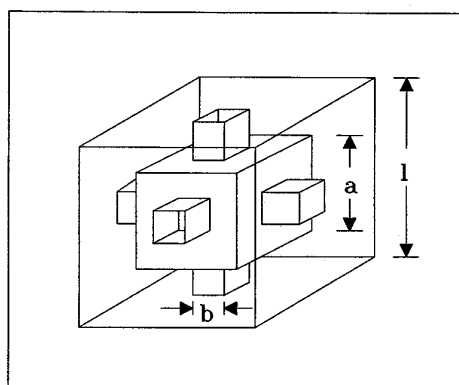


Figure 1. Idealization of the local geometry of secondary pore space.

block, a centered cubic vug of side length $\alpha(x)$ is cut out, where $0 \leq \alpha(x) \leq l$ (see Fig. 1). Now, a cylindrical pore of square cross-section with side length $\beta(x)$, where $0 \leq \beta(x) \leq \alpha(x)$, is drilled from each of the faces of the block toward the central vug. This process creates a cubic vug pore body and six vug pore throats within each block of porous matrix of size l that has non-zero vuggy porosity. The vuggy porosity at this scale may be expressed in terms of the vug pore body size $\alpha(x)$, the size l of the block and the vug pore throat to pore body aspect ratio R ($0 \leq R \leq 1$) as follows:

$$\phi_v(x) = (1-3R^2)[\alpha(x)/l]^3 + 3R^2[\alpha(x)/l]^2 \quad (2)$$

This equation may be solved for $\alpha(x)$ given the values of R , l and $\phi_v(x)$ (see Fig. 2). The parameter R accounts for the fact that each vug may be accessible through constrictions in the secondary pore space, which are here assumed to be a constant fraction of the local vug size $\alpha(x)$, *i.e.*, $R = \beta(x)/\alpha(x)$. The simple construction outlined above enables the calculation of a capillary pressure for non-wetting phase invasion into each block through secondary pore space features (vug pore throats) of size $\beta(x)$, denoted by $P_c(\beta(x))$, as a function of local vug porosity $\phi_v(x)$ and vug size aspect ratio R .

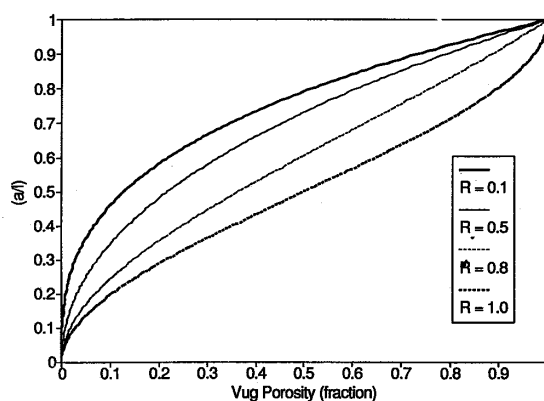


Figure 2. Relative vug size as a function of local vug porosity.

Primary drainage in a dual-network model may be simulated using invasion percolation with the following modifications. The capillary pressure required for non-wetting phase invasion into each block of size l may be determined by either the size of vug pore throats, $\beta(\mathbf{x})$, or the breakthrough capillary pressure of the matrix, $\{P_c^o\}_m$. For matrix with uniform properties, this may be expressed as

$$P_c^o(\mathbf{x}) = \begin{cases} \{P_c^o\}_m & ; \phi_v(\mathbf{x}) \leq \phi_v^{(crit)} \\ P_c(\beta(\mathbf{x})) & ; \phi_v(\mathbf{x}) > \phi_v^{(crit)} \end{cases}, \quad (3)$$

where $\phi_v^{(crit)}$ is a critical value of the local vug porosity $\phi_v(\mathbf{x})$ for which $P_c(\beta(\mathbf{x})) = \{P_c^o\}_m$ and corresponds to a critical constriction of size $\beta^{(crit)}$ in the secondary pore space. The value of $\{P_c^o\}_m$ may be calculated from the known matrix permeability k_m . The value of $\phi_v^{(crit)}$ may then be obtained from knowledge of $P_c(\beta^{(crit)})$, R and l .

A block of size l is considered “open” to an invading non-wetting phase if the externally applied pressure exceeds $P_c^o(\mathbf{x})$. An “open” block is invaded if it is adjacent to a block already invaded by the non-wetting phase. For values of the externally applied pressure that are smaller than $\{P_c^o\}_m$, blocks may become accessible through secondary pore space features only (*i.e.*, vug pore throats). Accordingly, clustering of the “open” blocks in this range of capillary pressures can be employed to determine the accessibility of the secondary pore network. Since this network may be partially disconnected, Eq. (1) is employed to determine the existence of a connection between two neighboring “open” blocks with vuggy porosity $\phi_v(\mathbf{x})$ and $\phi_v(\mathbf{x}^*)$. If a connection does not exist the blocks are not clustered together. Matrix pores in blocks that become accessible when the externally applied pressure is less than $\{P_c^o\}_m$ cannot be invaded by the non-wetting phase; only the secondary pore space (vugs) in these blocks is penetrated under these conditions.

For every value of the externally applied pressure that is greater than $\{P_c^o\}_m$, blocks are accessible through matrix pores. If the matrix properties are uniform, all blocks are immediately invaded by the non-wetting phase when the externally applied pressure exceeds $\{P_c^o\}_m$. In this case, the secondary pore space in all blocks is completely invaded, whereas the network of matrix pores is invaded to an extent dictated by the drainage capillary pressure curve of the matrix. Although uniform matrix properties are assumed here, this assumption can be easily relaxed by letting $\{P_c^o\}_m = \{P_c^o\}_m(\mathbf{x})$ in Eq. (3) (Ioannidis *et al.*, 1996). The non-wetting phase saturation in each accessible block, $S_{nw}(\mathbf{x})$, may be computed as follows:

$$S_{nw}(\mathbf{x}) = \frac{\phi_v(\mathbf{x}) + [1 - \phi_v(\mathbf{x})]\phi_m S_{nwm}}{\phi_v(\mathbf{x}) + [1 - \phi_v(\mathbf{x})]\phi_m}, \quad (4)$$

where $S_{\text{nw}} = S_{\text{nw}}(P_c)$ is the non-wetting phase saturation in the matrix pore network. The effective non-wetting phase saturation in the model is computed as the weighed average of block saturations, where the weighing factor is the total block porosity.

Network Simulation Results and Discussion

A case study of primary drainage in a dual-network model was conducted using the vug porosity distribution shown in Fig. 3. This distribution is similar to the one reported by Hicks *et al.* (1992). A model porous medium consisting of 30^3 blocks of size $l = 10$ mm each was simulated. The porous matrix was assumed to have a uniform porosity $\phi_m = 0.03$ and permeability $k_m = 2.72$ mD, corresponding to a mercury-air breakthrough capillary pressure $\{P_c^o\}_m = 59.2$ psi. The drainage capillary pressure curve of the matrix is given in Fig. 4. Vuggy porosity values were randomly assigned to each block in an uncorrelated manner. Thus, a model porous medium was created with average vug porosity $\langle\phi_v\rangle = 0.110$ and total porosity $\phi = 0.137$. Four simulations of primary drainage were performed to investigate the effect of model parameters ω and R .

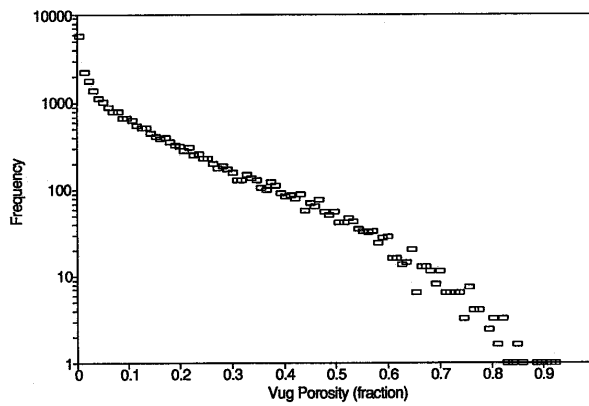


Figure 3. Local vug porosity distribution used in simulations.

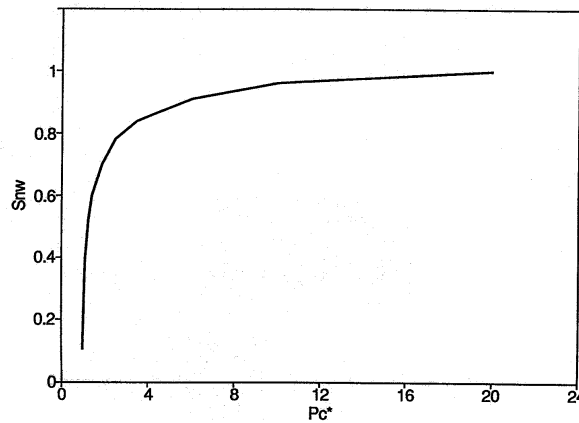


Figure 4. Matrix drainage capillary pressure curve used in simulations in terms of the reduced capillary pressure $P_c^* = P_c / \{P_c^o\}_m$.

The effect of secondary pore network connectivity on the large-scale capillary behavior of a dual-porosity system is illustrated in Fig. 5(i). For a given distribution of vuggy porosity, higher values of ω result in higher connectivity (cf. Eq. (1)) and for $\omega = 1$ one has exactly six connections per block, that is a simple cubic network of vugs. Incomplete connectivity for $\omega < 1$ is measured by the ratio f_c of the number of existing connections to the number of connections in a cubic network of vugs. For $\omega = 0.7, 0.8$ and 0.97 we find $f_c = 0.170, 0.298$ and 0.832 , respectively. Apparently, the secondary pore network percolates for all values of ω considered, even when its connectivity is rather tenuous ($\omega = 0.7; f_c = 0.170$). As a consequence, the large-scale breakthrough capillary pressure is determined by the accessibility of the secondary pore network and is found to be $\{P_c^o\} = 1.16$ psi for $\omega = 0.7$ or 0.8 and $\{P_c^o\} = 0.458$ psi for $\omega = 0.97$. Although the percolation threshold p_{sc} (*i.e.*, number fraction of blocks that must be “open” for a sample-spanning cluster of secondary pores to exist) is equal to 0.818 in each case, the number fraction Y_s of blocks accessible through secondary pore space features at breakthrough conditions is different. For values of $\omega = 0.7, 0.8$ and 0.97 we find $Y_s = 0.04, 0.23$ and 0.24 , respectively. This finding suggests that for $\omega = 0.7$ at least one sample-spanning pathway through secondary pores is also part of the percolation cluster for $\omega = 0.8$. As seen in Fig. 5(i), the simulated drainage capillary pressure curve consists essentially of two parts, corresponding to non-wetting phase penetration into the secondary and matrix pore networks, respectively. A larger fraction of vugs are accessible as the connectivity of the secondary pore space increases, hence the different plateau’s of non-wetting phase saturation. Additionally, the capillary pressure at which the same value of saturation is attained decreases with increasing connectivity of the secondary pore network. Decreasing the value of aspect ratio R has the effect of decreasing the size of the constrictions in the secondary pore network through which vug communication takes place. Therefore the capillary pressure for non-wetting phase invasion into the network of vugs also increases, as shown in Fig. 5(ii).

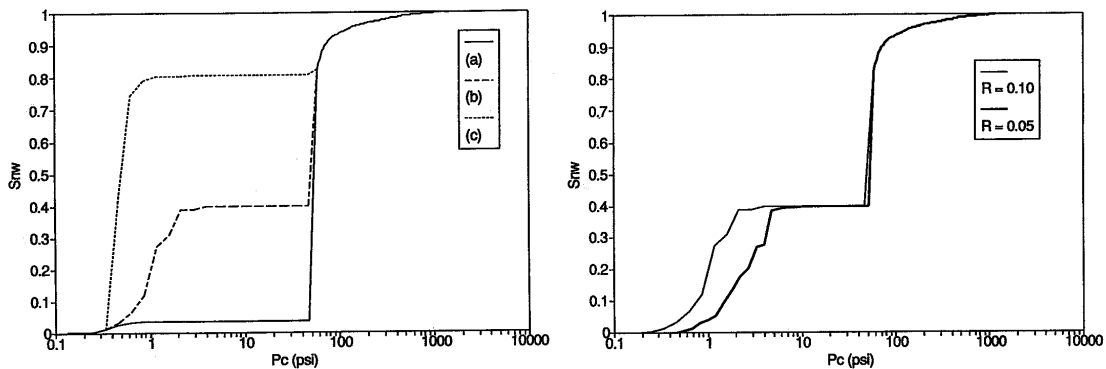


Figure 5. (i) Effect of vug connectivity on primary drainage: (a) $\omega = 0.7$, (b) $\omega = 0.8$, (c) $\omega = 0.97$. (ii) Effect of channel-vug size aspect ratio R on primary drainage.

The model calculations presented above illustrate the widely diverse capillary behavior that can be reproduced by dual-network models. In particular, non-wetting phase breakthrough during primary drainage in vuggy carbonates can take place at values of capillary pressure much lower than the breakthrough capillary pressure of the matrix. Also, depending on the degree of interconnectedness of the secondary pore network and the distribution of vuggy porosity, very different values of non-wetting phase saturation can be attained in carbonates characterized by the same value of breakthrough capillary pressure.

Core Analysis Results and Discussion

Core analysis tests on several samples were performed in order to gain insight into the transport and capillary behavior of vuggy carbonates. The core material consisted of 17 core plugs (3.9-4.5 cm in diameter and 6.7-7.6 cm in length) obtained from full diameter cores by drilling perpendicularly to the core axis. The sample origin is the Upper Guelph (Middle Silurian) carbonate sediment reservoir of Fletcher field (Chatham, Ontario). All samples are intercrystalline dolomites, most containing numerous vugs ranging in size from about 0.2 to more than 5 mm. All samples were extracted with toluene in a Soxhlet apparatus prior to core analysis, although none of them contained oil. Measurements were made of porosity, permeability to nitrogen (Klinkenberg-corrected), brine (2% NaCl) and kerosene, formation factor, gas-brine breakthrough capillary pressure, resistivity index and brine saturation at gas breakthrough. Additionally, mercury porosimetry tests were performed on small cubes (about 1 cm³ in volume) cut from several cores. All except one of the cubes' faces were covered with epoxy resin to minimize surface penetration effects.

The formation resistivity factor values for all samples tested are plotted against porosity in Fig. 6. These data are well represented by the following equation:

$$F = 1.15\phi^{-1.72} \quad (5)$$

The values of $a = 1.15$ and $m = 1.72 (\pm 0.15)$ obtained for the prefactor and cementation exponent, respectively, are in agreement with literature data for intergranular porous media. One would expect values of the cementation exponent in excess of two for porous media with significant amounts of disconnected vuggy porosity. Although such an expectation is borne out by both theory (Ioannidis *et al.*, 1997) and experiment (Focke and Munn, 1987), it is not met by the samples studied.

The nitrogen-brine breakthrough capillary pressure of ten core samples was determined using a gas injection technique. A fully saturated core was placed in a core holder and nitrogen gas was slowly injected using a positive displacement high-pressure pump. The gas pressure at the sample inlet was continuously monitored using a pressure transducer and the signal fed to a microcomputer. Flow rates corresponding to injection pressure increases of less than 0.001 psi/min were used. The point of gas breakthrough was identified on the inlet pressure vs. time curves with a sharp decline in inlet pressure.

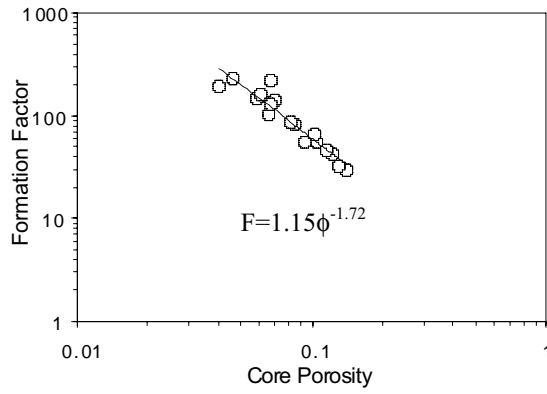


Figure 6. Formation factor of Fletcher field carbonates.

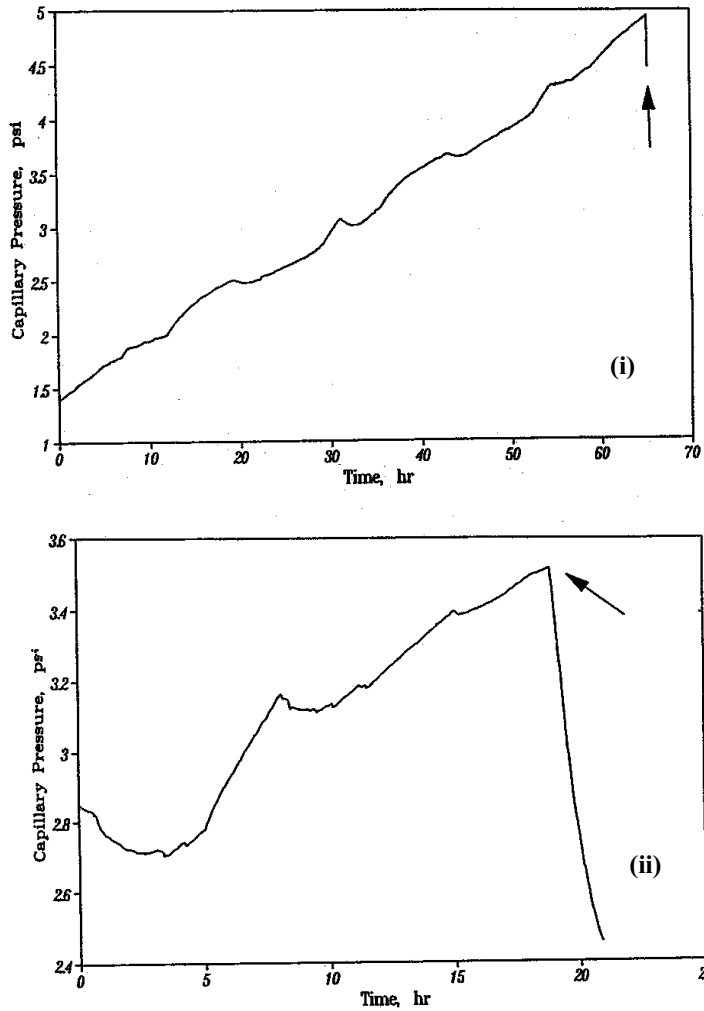


Figure 7. Apparent capillary pressure vs. time: (i) Core #9, $\phi = 0.115$, $k_{\text{brine}} = 0.543$ mD;
(ii) Core #4, $\phi = 0.07$, $k_{\text{brine}} = 0.728$ mD.

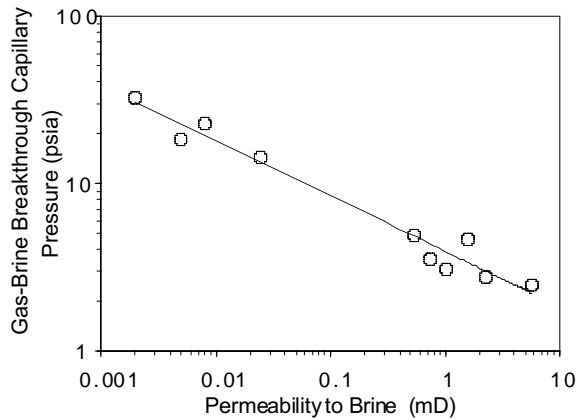


Figure 8. Correlation between permeability to brine and nitrogen-brine breakthrough capillary pressure for Fletcher field carbonates.

The breakthrough capillary pressure was estimated as the highest pressure attained before gas breakthrough. Figures 7(i)-(ii) illustrate the pressure responses of the least and most vuggy sample, respectively. The pressure response curve of the vuggiest sample consists of a number of prominent “peaks” and “valleys” associated with penetration of vugs by the gas. The nitrogen-brine breakthrough capillary pressure measurements are plotted against brine permeability in Fig. 8. These data are well represented by the following equation:

$$P_c^o = 3.66k^{-0.34} \quad (6)$$

where P_c^o is in psi and k is in mD. Similar relationships have been obtained for homogeneous sandstones and are theoretically justified within the framework of percolation theory (Ioannidis and Chatzis, 1993). The important difference between those results and the ones obtained here is in the value of the prefactor in Eq. (6), which is about 16.8 for several sandstones. The significantly lower values of breakthrough capillary pressure observed for vuggy carbonates indicate that the breakthrough pathways in these samples consist of much larger, but not highly connected pores.

The measurements of resistivity index and gas saturation at conditions of gas breakthrough are summarized in Table 1. Gas saturations vary from about 20%, a value typical of homogeneous sandstones, to more than 40% for the most vugular samples. High values of the resistivity index at breakthrough conditions imply a rather significant contribution of the breakthrough pathways to the overall electrical conductance of the sample. The results obtained suggest the existence of a sample-spanning network of secondary pores of relatively large size that are accessible at conditions of gas breakthrough.

Mercury porosimetry results obtained from four cubic samples cut from core #9 are shown in Fig. 9. These results indicate that the structure of this material is uniform at the scale of 1 cm³. A very different picture was obtained from samples cut from core #4, as shown in Fig. 10. Here, several saturation plateaus are observed at different capillary pressures during mercury injection. Differences in saturation hysteresis between primary drainage and imbibition are due to sample heterogeneity at the scale of investigation. The sample volume (*ca.* 1 cm³) is clearly too small to infer the capillary pressure vs. saturation relationship at the core plug scale from these tests.

Table 1. Summary of core analysis measurements

Core #	P_c^o (air-brine) [psi]	S_{nw} (%) at breakthrough	Resistivity Index at breakthrough	F	ϕ	k_{brine} [mD]
1	18.1	-	1.57	147.1	0.058	0.005
2	4.60	47.7	2.92	161.9	0.061	1.60
3	22.8	27.8	1.87	189.7	0.040	0.008
4	3.52	40.6	4.22	140.7	0.070	0.73
8	2.46	20.5	1.75	32.5	0.131	5.70
9	4.95	23.1	2.67	46.4	0.115	0.54
11	32.4	43.1	2.40	226.1	0.046	0.002
12	2.78	29.7	3.33	81.3	0.085	2.31
14	14.3	25.7	1.82	105.1	0.066	0.025
15	3.08	37.0	2.80	85.3	0.081	1.02

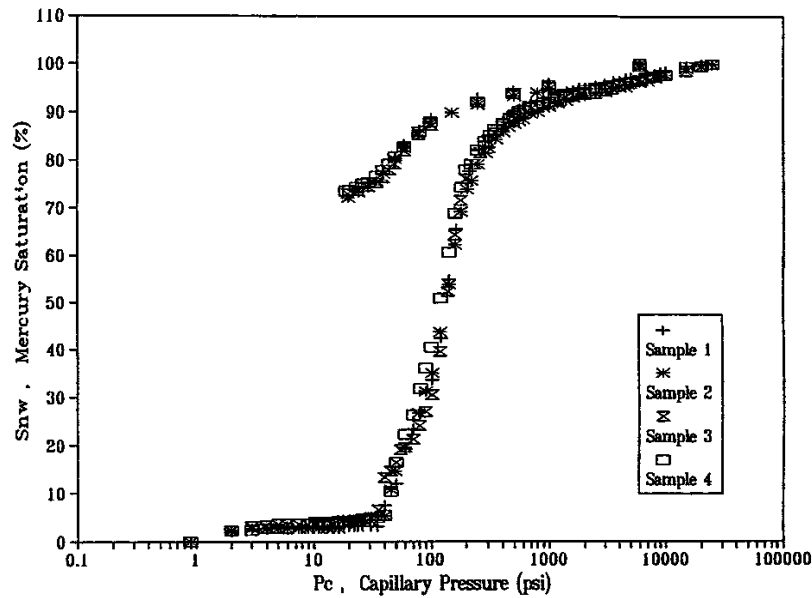


Figure 9. Mercury-air drainage and imbibition capillary pressure curves of four samples from core #9.

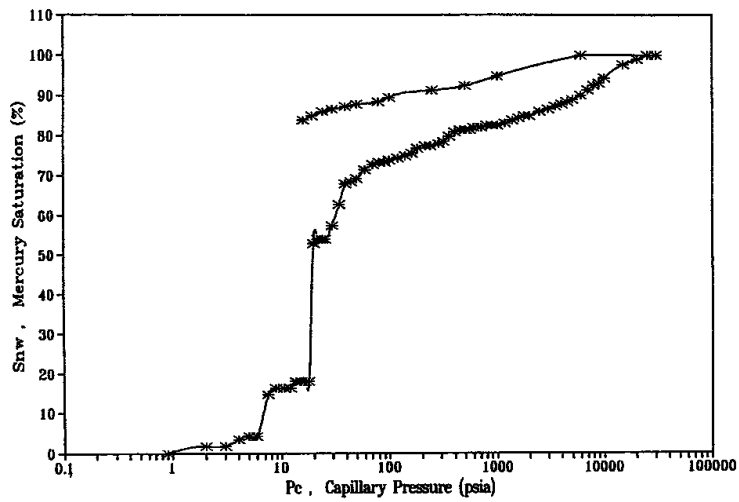
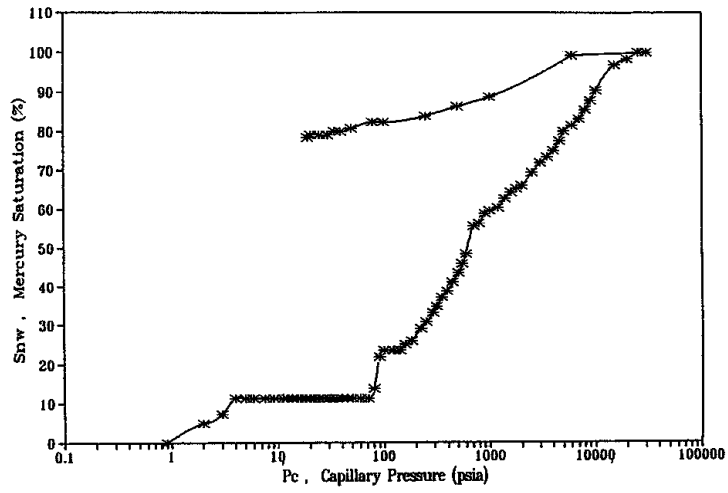
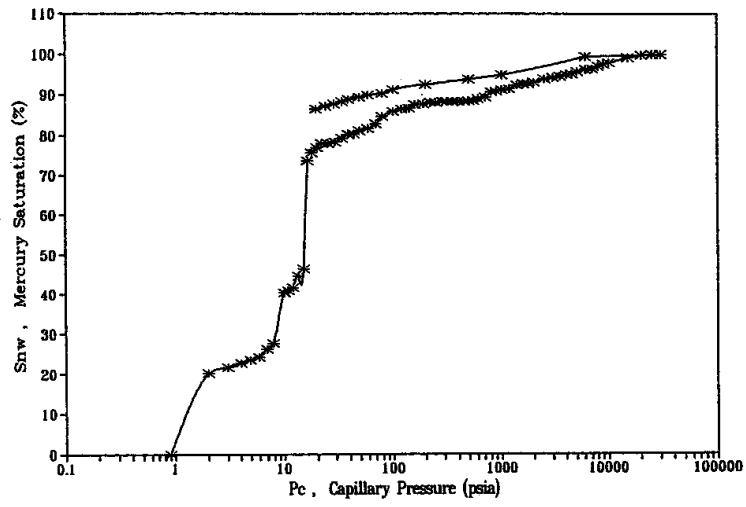


Figure 10. Mercury-air drainage and imbibition capillary pressure curves of three samples from core #4.

Conclusions

Core analysis results obtained from a suite of vuggy carbonate core samples provide qualitative evidence in support of a dual-network model of pore structure. The model highlights the importance of interconnectedness of the secondary pore space in determining fluid distributions under capillary equilibrium. It can quantitatively accommodate many aspects of carbonate pore structure, including distribution and spatial order of matrix properties, distribution and spatial order of vuggy porosity, partial interconnectivity of the secondary pore space and vug connectivity through constrictions in the secondary pore space continuum (vug pore throats). A versatile dual-network model should prove useful in elucidating the capillary and electrical properties of vuggy carbonates.

References

- Focke, J.W. and Munn, D., "Cementation Exponents in Middle Eastern Carbonate Reservoirs", *SPE Formation Evaluation*, (1987) **2**, 2, 155.
- Gleeson, J.W., Woessner, D.E. and Jordan, C.F., "NMR Imaging of Pore Structures in Limestones", *SPE Formation Evaluation*, (1993) **8**, 2, 123.
- Hicks, P.J., Deans, H.A. and Narayanan, K., "Distribution of Residual Oil in Heterogeneous Carbonate Cores Using X-Ray CT", *SPE Formation Evaluation*, (1992) **7**, 3, 235.
- Ioannidis, M.A. and Chatzis, I., "Network Modeling of Pore Structure and Transport Properties of Porous Media", *Chemical Engineering Science*, (1993) **48**, 5, 951.
- Ioannidis, M.A., Chatzis, I. and Dullien, F.A.L., "Macroscopic Percolation Model of Immiscible Displacement: Effects of Buoyancy and Spatial Structure", *Water Resources Research*, (1996), **23**, 3297-3310.
- Ioannidis, M.A., Kwiecien, M.J. and Chatzis, I., "Electrical Conductivity and Percolation Aspects of Statistically Homogeneous Porous Media", *Transport in Porous Media*, (1997), **29**, 61-83.
- Kamath, J., Xu, B., Lee, S.H. and Yortsos, Y.C., "Use of Pore Network Models to Interpret Laboratory Experiments on Vugular Rocks", *Journal of Petroleum Science and Engineering*, (1998), **20**, 109-115.
- Lucia, F.J., "Petrophysical Parameters Estimated from Visual Descriptions of Carbonate Rocks: A Field Classification of Carbonate Pore Space", *Journal of Petroleum Technology*, (1983), **35**, 3, 629.